J Mater Sci: Mater Med (2011) 22:2187–2196
DOI 10.1007/s10856-011-4415-3

Mg- and Zn-modified calcium phosphates prepared by biomimetic precipitation and subsequent treatment at high temperature

D. Rabadjieva · S. Tepavitcharova · R. Gergulova · K. Sezanova · R. Titorenkova · O. Petrov · E. Dyulgerova

Received: 22 June 2011 / Accepted: 6 August 2011 / Published online: 26 August 2011

Abstract Powders of magnesium-modified as well as zinc-modified calcium phosphates (Me-β-TCP and HA) with a $(Ca^{2+}+Mg^{2+}+Zn^{2+}+Na^{+}+K^{+})/P$ ratio of 1.3–1.4 and various $Me^{2+}/(Me^{2+}+Ca^{2+})$ ratios (from 0.005 to 0.16) were prepared in biomimetic electrolyte systems at pH 8, mother liquid maturation and further syntering at 600–1000°C. Some differences in zinc and magnesium modifications have been prognosed on the basis of thermodynamic modeling of the studied systems and explained by the Mg^{2+} and Zn^{2+} ion chemical behaviour. The temperature as well as the degree of Zn^{2+} and Mg^{2+} ions substitutions were found to stabilize the β-TCP structure and this effect was more prononced for zinc. Thus, zinc-modified β-TCP powders consisting of idiomorphic crystals were obtained through sintering of Zn^{2+} ion substituted calcium phosphates precursors at 800–1000°C. The Mg^{2+} ion substitution leads to obtaining magnesium-modified β-TCP with spherical grains.

D. Rabadjieva (✉) · S. Tepavitcharova · R. Gergulova · K. Sezanova
Institute of General and Inorganic Chemistry, Bulgarian Academy of Sciences, Acad. G. Bontchev Str., Bl.11, 1113 Sofia, Bulgaria
e-mail: didiarab@svr.igic.bas.bg

R. Titorenkova · O. Petrov
Institute of Mineralogy and Crystallography, Bulgarian Academy of Sciences, Acad. G. Bontchev Str., Bl.107, 1113 Sofia, Bulgaria

E. Dyulgerova
Dental Medicine Faculty, University of Medicine, 1 G. Sofiiski Str, 1431 Sofia, Bulgaria

1 Introduction

Ion-substituted non-stoichiometric nano-sized calcium orthophosphates, mainly with apatite structure, build up the inorganic component of the biological mineralized structures. The main ion substitutes are the ions Na^{+}, K^{+}, Mg^{2+}, Fe^{2+}, Zn^{2+}, CO_3^{2-}, Cl^{-} and F^{-} [1, 2] and they differ in variety and amount depending on many factors, such as genetic, individual characteristics and internal environment of the mineralized structures.

Ion modified calcium phosphate-based ceramics and cements [3–13] have been developed to simulate the composition of the mineral component of bone tissues and to strengthen some specific biologically important behaviors, thus to be prospective materials for bone reconstruction and remodeling. Mg and Zn are preferable among all the substitutes [5–13] in the biological apatites as they are essential for the organisms. Thus, the biologically active Mg plays an important role in the formation and initial growth of the bone tissue [5]. Zn is an important element in the natural biological growth and development of the skeletal system [12]. Moonga and Dempster [13] founded that Zn inhibits osteoclast differentiation and promotes osteoblast activity. Most often, bioceramics based on hydroxyapatite (HA), tricalcium phosphate (α- or β-TCP) or bi-phase HA/β-TCP are used [14–16] due to their good osteoconductivity, physiological tolerance, biocompatibility, etc. [17, 18]. Practically insoluble mono-phase bioceramics of HA that have a long-term stability do not actively participate in the process of bone remodeling however, at the contact with body fluids they are involved in the formation of a surface layer of bone-like apatite. The mono-phase α-TCP and β-TCP display high reactivity and they degrade rapidly in vitro and in vivo [19, 20]. Mg and Zn doped TCP ceramics was found to posses lower

solubility than pure ones and hence reduce the resorption rate [10]. Bi-phase mixtures of HA and β-TCP ceramics were developed in order to improve the biological behavior of the mono-phase materials [21].

The aim of this work was to trace and explain the differences in the biomimetic precipitation of magnesium- and of zinc-modified calcium phosphate precursors in simulated body fluid electrolyte systems and their subsequent temperature (600–1000°C) phase transformations by application of chemical, XRD, FTIR, and SEM methods and thermodynamic modeling.

2 Materials and methods

2.1 Materials—simulated body fluids

The popular conventional simulated body fluid (SBFc) [22] (Table 1) was used to assure electrolyte medium in this study. Modified calcium-free conventional simulated body fluid (SBFc-*Cam*) was used as a solvent for K_2HPO_4 (Solution 1, Table 1) and modified phosphorous-free conventional simulated body fluid (SBFc-*Pm*) was used as a solvent for $CaCl_2$ (Solution 2, Table 1), for $ZnCl_2$ (Solution 3, Table 1), and for $CaCl_2$ and $MgCl_2$ (Solution 4, Table 1), respectively, thus preliminary precipitation was avoided. All the simulated body fluids used in the experiments (Table 1) were prepared by successive mixing of preliminary prepared solutions of KCl, NaCl, $MgCl_2{\cdot}6H_2O$, $CaCl_2{\cdot}2H_2O$, $ZnCl_2{\cdot}1.5H_2O$, $NaHCO_3$, Na_2SO_4, and K_2HPO_4 salts in distilled water. The pH of the solutions was adjusted to 7.2–7.4 using 0.1 M HCl or 0.05 M Tris (hydroxymethyl) aminomethane. Analytical reagents A.R. were used.

2.2 Synthesis and phase transformations

Magnesium-modified as well as zinc-modified calcium phosphate precursors with varying $Me^{2+}/(Ca^{2+}+Me^{2+})$ ratio ($Me^{2+} = Mg^{2+}$, Zn^{2+}) from 0.005 to 0.16 (Table 2) were biomimetically synthesized in electrolyte medium of SBF and a glycine buffer [23] at pH 8 and room temperature. The method of continuous co-precipitation was applied and all reagents (Solution 1 and Solution 2 for SBFc, Solutions 1–3, for Zn- and Solution 1 and Solution 4 for Mg-modifications (Table 1)) were added to a glycine buffer medium with a rate of 3 ml/min assuring continuous precipitation at a constant $(Ca^{2+}+Me^{2+})/P$ ratio of 1.67 and keeping pH 8 by 1 M NaOH.

The precipitates were matured in the mother liquid for 24 h at room temperature and then the thick suspensions were subjected to gelling with xanthan gum, lyophilized at −56°C, washed (solid-to-water-ratio 1:100), and secondary lyophilized.

The dry precursors were sintered at 600, 800 and 1000°C and atmospheric pressure in high-temperature furnace, type VP 04/17 of LAC Ltd Company. The working regime was heating with rate 3°C/min till the desired temperature and keeping it constant for 1 h.

2.3 Characterization

2.3.1 Chemical analysis

The sum of Ca^{2+} and Mg^{2+} ions in the solid samples was determined complexometrically with EDTA at pH 10. The concentrations of Zn^{2+}, Mg^{2+}, K^+ and Na^+ ions were analyzed by a TERMO M5 atomic absorption spectrometer and the concentrations of $P\text{-}PO_4^{3-}$ and Cl^- ions were analyzed spectrophotometrically by NOVA 60 equipment using Merck and Spectroquant® test kits.

Table 1 Inorganic composition of human plasma and simulated body fluids (SBF) (mmol dm^{-1})

Composition	Human plasma [22]	SBFc [22]	*SBFc-Cam* (Solution 1)	*SBFc-Pm* (Solution 2)	*SBFc-Pm* (Solution 3)	*SBFc-Pm* (Solution 4)
Na^+	142.0	142.0	141.9	141.9	141.9	141.9
K^+	5.0	5.0	506.4	3.0	3.0	3.0
Mg^{2+}	1.5	1.5	1.5	1.5	1.5	1.5 + x
Ca^{2+}	2.5	2.5	–	418.9 − x		418.9 − x
Zn^{2+}	–	–	–		x	
Cl^-	103.0	147.8	142.8	975.6 − 2x	142.8 + 2x	975.6
SO_4^{2-}	0.5	0.5	0.5	0.5	0.5	0.5
HCO_3^-	27.0	4.2	4.2	4.2	4.2	4.2
HPO_4^{2-}	1.0	1.0	251.7	–	–	–

Note: $0 < x < 83.8$ mmol/l that corresponds to $Me^{2+}/(Me^{2+}+Ca^{2+}) = 0.2$

Table 2 Ion content of the magnesium- and zinc-modified calcium phosphates and their initial solutions

Sample	Liquid phase	Solid phase						
	$Me^{2+}/(Me^{2+}+Ca^{2+})$ in initial solutions	$Me^{2+}/(Me^{2+}+Ca^{2+})$	$(Ca^{2+}+Mg^{2+}+Zn^{2+}+Na^{+}+K^{+})/P$	Zn^{2+}, mmol/g	Mg^{2+}, mmol/g	Na^{+}, mmol/g	K^{+}, mmol/g	Cl^{-}, mmol/g
SBF-modified calcium phosphate								
P0	0	0.005	1.33	–	0.04	0.05	0.01	<0.05
Zinc-modified calcium phosphates								
Zn1	0.01	0.01	1.31	0.09	0.03	0.03	0.01	<0.05
Zn5	0.05	0.05	1.35	0.41	0.04	0.05	0.02	<0.05
Zn10	0.10	0.10	1.34	0.90	0.06	0.02	0.01	<0.05
Zn13	0.13	0.13	1.40	1.19	0.05	0.08	0.02	<0.05
Magnesium-modified calcium phosphates								
Mg2	0.03	0.02	1.36	–	0.21	0.05	0.02	<0.05
Mg5	0.10	0.05	1.35	–	0.45	0.08	0.01	<0.05
Mg10	0.13	0.10	1.33	–	0.85	0.06	0.02	<0.05
Mg16	0.20	0.16	1.38	–	1.45	0.04	0.02	<0.05

2.3.2 X-ray diffraction analysis

The polymorphous phase transformations of the amorphous and high temperature treated calcium phosphates were determined by a Bruker D8 advance XRD apparatus operating at 40 kV and 40 mA with CuK_{α} radiation and SolX detector within the 2θ range 10–90°2θ, step 0.04°2θ and counting time of 1 s/step. The phase analysis was performed comparing the experimentally measured diffraction lines with patterns from the PDF database of ICDD. The principal calcium phosphate phases in the studied samples corresponded to whitlockite ($Ca_3(PO_4)_2$—PDF # 09-0169), hydroxyapatite ($Ca_5(PO_4)_3(OH)$—PDF # 09-0432), ($Ca_{19}Zn_2(PO_4)_{14}$—PDF# 48-1196) and ($Ca_{2.81}Mg_{0.19}(PO_4)_2$—PDF# 70-0682).

2.3.3 IR spectroscopy

The IR transmission spectra of solid samples were collected by a Tensor 37 FTIR spectrometer in the 400–4000 cm^{-1} spectral range with a 4 cm^{-1} spectral resolution, after averaging 72 scans on standard KBr pallets. OPUS 5.5 was used for the evaluation of the spectra. The spectra were baseline corrected via rubber band correction, normalized to the corresponding maximum intensity and smoothed at 5 points.

2.3.4 Morphology studies—SEM images

The sintered samples were sputter-coated with gold. The morphology and microstructure were observed using scanning electron microscope JEOL JSM-5510 equipment operating at voltage of 10 kV. ImageJ software was used to analyze the average grain size.

2.4 Thermodynamic simulations

Ion-association model (computer program PHREEQCI v.2.14.3.) was used to simulate the precipitation process [24]. All possible association/dissociation and dissolution/crystallization processes in SBF electrolyte solutions were taken into account. The complex formation and salt precipitation were defined by a mass-action expression with the appropriate formation constant or solubility product. The activity coefficients of all possible simple and complex species were calculated using the extended Debye-Hueckel theory. An updated database [25] was used.

The saturation indices (SI) (Eq. 1) were calculated under the experimental conditions as an indicator for possible salts crystallization.

$$SI = \lg(IAP/K), \quad (1)$$

where IAP is an ion activity product, and K is a solubility product.

Data by Fernández [26] and Dorozhkin [1] for solubility products of calcium phosphates were used for the calculation. Data for zinc phosphate salts were limited up to $Zn_3(PO_4)_2 \cdot 4H_2O$.

3 Results and discussion

The ion-modified calcium phosphates are mixed crystals (non-stoichiometric compounds), where a part of the ions building the crystal unit cell are substituted by other ions. The ability of the admixture ion to accept the coordination of the substituted ion determines the substitution degree. In this study we discuss magnesium and zinc modification of

calcium phosphates due to Me^{2+} ion substitution, ion incorporation and co-crystallization. Thus, the prepared magnesium modified calcium phosphates had $Mg^{2+}/(Mg^{2+} + Ca^{2+})$ ratio even higher than the theoretically calculated value (0.15) of possible Me^{2+} ion substitution [27]. The biomimetic approach for precipitation of this type of mixed crystals was applied. It includes precipitation in electrolyte medium of simulated body fluid (SBF) that becomes a modern way for preparation of bioactive materials [28–30] with composition and properties close to the biological hard tissues. Modified conventional simulated body fluids (Table 1) were used in the experiments in order to ensure ion modification of all calcium phosphate precursors with Na^+ (0.02–0.08 mmol/g), K^+ (0.01–0.02 mmol/g, Mg^{2+} (0.04 mmol/g) and Cl^- (below 0.05 mmol/g) ions (Table 2).

Poorly soluble salts, such as calcium phosphates and their mixed crystals usually are prepared by adding the precipitant in the solutions, thus inhomogeneous precipitates often appear. Chemical, crystal chemical, kinetic and thermodynamic factors determine the crystallization of the salts in the water-salt systems. Recently, we have found that the kinetic factors were dominant at quick precipitation in biomimetic conditions and metastable XRD amorphous calcium deficient phosphate (ACP) was precipitated as a first stage in the solutions with initial Ca/P ratio of 1.67, instead of thermodynamically stable HA, $Ca_{10}(PO_4)_6(OH)_2$ [31]. In this study, working in the systems SBF (Na^+, K^+, Mg^{2+}, Ca^{2+}, Cl^-, SO_4^{2-}, CO_3^{2-}, HPO_4^{2-})–$CaCl_2$–$ZnCl_2$–K_2HPO_4–KOH and SBF (Na^+, K^+, Mg^{2+}, Ca^{2+}, Cl^-, SO_4^{2-}, CO_3^{2-}, HPO_4^{2-})–$CaCl_2$–$MgCl_2$–K_2HPO_4–KOH we have established in analogy with Bigi et al. [32], that the presence of Zn^{2+} or Mg^{2+} ions in the reaction solution also inhibit the crystallization of HA. Thus, we synthesized XRD amorphous magnesium- as well as zinc-modified calcium phosphates precursors with calcium deficiency and varying $(Ca^{2+}+Mg^{2+}+ Zn^{2+} + Na^+ + K^+)/P$ ratios from 1.31 to 1.4 (Table 2) that further re-crystallized to calcium deficient carbonate apatite (Fig. 1). IR spectra of the matured product exhibit an intense peak around 1064 cm^{-1}, which is due to antisymmetric P–O stretching (ν_3) vibrations and at 570 cm^{-1} due to phosphate bending vibrations (Fig. 1). The peaks in the 1420–1503 cm^{-1} spectral range are characteristic of C–O stretching vibrations (ν_3), whereas the peak at about 870 cm^{-1} is generated by the bending mode of carbonate groups. The method used of continuous co-precipitation allows keeping equal doses of the reagents during the precipitation process, thus ensuring conditions for chemically homogenous precipitation. Precipitation, co-precipitation, ion substitution and ion inclusion reactions take place simultaneously in the complicated electrolyte system of SBFs. The presence of different cations and anions is mainly responsible for the ions substitutions and cationic deficiency of the precipitated ACP. According to Posner et al. [33, 34] Posner's clusters with a formula $Ca_9(PO_4)_6$ (Ca/P = 1.5) are formed as a first step in the mechanism of ACP formation. The CO_3^{2-} ions from the solution compete with and partially replace the PO_4^{3-} ions in the structure following, however, the rule for electrostability that results in a structure with Ca vacancies and lower Ca/P ratio.

As the modifying ions have an ionic radius and electrical charge closer to these of Ca^{2+} ions they easily will be incorporated in the calcium phosphate structure. The substitution with Zn^{2+} and Mg^{2+} ions is preferential than the one with Na^+ and K^+ ions because not only of geometrical reasons (differences in ionic radiuses [35]) but also of electrostability. Our studies have found difference in substitution ability of Zn^{2+} and Mg^{2+} ions. The results (Table 2) showed that all Zn^{2+} ions and only about half of the Mg^{2+} ions from the reaction solutions were incorporated in the precipitated ACP. We elucidate this difference by the different chemical behavior of Zn^{2+} and Mg^{2+} ions in the studied electrolyte systems that can be explained by the factor "softness-hardness" and by the Crystal Field Stabilization Energy (CFSE). The Pearson concept of "hard" and "soft" Lewis acids and bases [36] as well as the Klopman scale of hardness and softness [37] determine the type of ligands that form the metal complexes in the water systems under consideration. According to them, "soft acids" coordinate predominantly "soft bases" and "hard acids" predominantly "hard bases". Mg is a "hard acid", while Zn is a "soft acid". In the simulated body fluids there are high concentrations of Cl^- ions, which are "softer bases" than H_2O, OH^-, PO_4^{3-}, SO_4^{2-}, HCO_3^- and HPO_4^{2-} ions are.

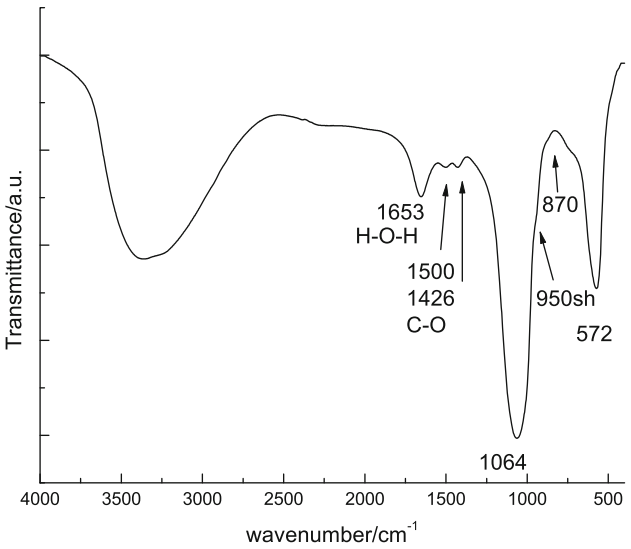

Fig. 1 FT IR spectra of ion-modified calcium phosphate precursor. Example of Zn-modified calcium phosphate $Zn^{2+}/(Zn^{2+}+Ca^{2+}) = 0.13$

Table 3 Saturation indices (SI) of solid phases in the studied systems

Solid phases	SBF–$CaCl_2$–K_2HPO_4–KOH	SBF–$CaCl_2$–$MgCl_2$–K_2HPO_4–KOH	SBF–$CaCl_2$–$ZnCl_2$–K_2HPO_4–KOH
NaCl	−3.18	−3.14	−3.21
$NaHCO_3$	−3.30	−3.31	−3.24
$Na_2CO_3·H_2O$	−7.85	−7.82	−7.77
$Na_2CO_3·10H_2O$	−5.97	−5.94	−5.87
$NaHCO_3·Na_2CO_3·2H_2O$	−10.27	−10.25	−10.13
Na_2SO_4	−6.80	−6.82	−6.70
$Na_2SO_4·10H_2O$	−5.44	−5.46	−5.33
$KMgPO_4·6H_2O$	−0.76	**0.60**	−1.11
$Mg(OH)_2$	−6.63	−5.18	−6.47
$MgCO_3$	−1.50	−0.11	−1.32
$MgCO_3·3H_2O$	−4.31	−2.92	−4.13
$Mg_5(CO_3)_4(OH)_2·4H_2O$	−14.94	−7.91	−14.07
$MgCO_3·Mg(OH)_2·3H_2O$	−6.42	−3.57	−6.08
$MgSO_4·7H_2O$	−6.16	−4.81	−5.96
$MgHPO_4·3H_2O$	−0.38	**0.95**	−0.60
$Mg_3(PO4)_2$	−1.60	**2.5**	−1.90
$Mg_3(PO_4)_2·8H_2O$	**0.27**	**4.36**	−0.03
$Mg_3(PO_4)_2·22H_2O$	−1.74	**2.35**	−2.02
$Ca(OH)_2$	−8.52	−8.45	−8.54
$CaCO_3$	**1.45**	**1.46**	**1.46**
$CaSO_4$	−1.76	−1.80	−1.74
$CaSO_4·2H_2O$	−1.53	−1.56	−1.50
$CaHPO_4$	**2.86**	**2.86**	**2.86**
$CaHPO_4·2H_2O$	**2.56**	**2.51**	**2.17**
$Ca_3(PO_4)_2$(am)	**6.66**	**6.62**	**5.85**
$Ca_8H_2(PO_4)_6·5H_2O$	**28.64**	**28.45**	**26.24**
$Ca_9Mg(HPO_4)(PO_4)_6$	**32.19**	**33.39**	**29.54**
$Ca_{10}(PO_4)_6(OH)_2$	**47.92**	**47.87**	**45.49**
$Zn(OH)_2$			−6.44
$ZnCO_3$			−5.35
$ZnCO_3·H_2O$			−5.10
$Zn_2(OH)_3Cl$			−12.28
$ZnSO_4·H_2O$			−13.98
$ZnSO_4·6H_2O$			−12.88
$ZnSO_4·7H_2O$			−12.64
$Zn_2(OH)_2SO_4$			−16.36
$Zn_3(PO_4)_2·4H_2O$			−9.49

Note: The digits in bold (SI > 0) correspond to the possible to co-crystallize solid phases

Although Zn^{2+} ions are "soft acid" they form negligible chloride complexes due to their CFSE = 0 (Crystal Field Stabilization Energy) and thus in the studied solutions existed mainly as free Zn^{2+} ions. Contrary, Mg^{2+} as a "hard acid" is coordinated preferentially by the "hard basis" H_2O molecules and existed mainly as $[Mg(H_2O)_6]^{2+}$ complexes. Thus, the lower substitution of Mg^{2+} ions is determined by the $[Mg(H_2O)_6]^{2+}$ complexes available in the solutions, which are too big for incorporation into the crystal structure of the calcium phosphate without being changed. The necessity of overcoming the energy barrier even for partial dehydration of the complexes $[Mg(H_2O)_6]^{2+}$ determines the low substitution rate of these ions.

Also, our thermodynamic calculations indicate the different character of Zn^{2+} and Mg^{2+} ions content in the calcium phosphate samples. The calculated saturation indices (SI) of solid phases (Table 3) possible to co-crystallize in the studied systems showed: (i) six calcium phosphates, only one magnesium phosphate ($Mg_3(PO_4)_2·8H_2O$), and $CaCO_3$ could co-precipitate in the non ion-modified SBF (their

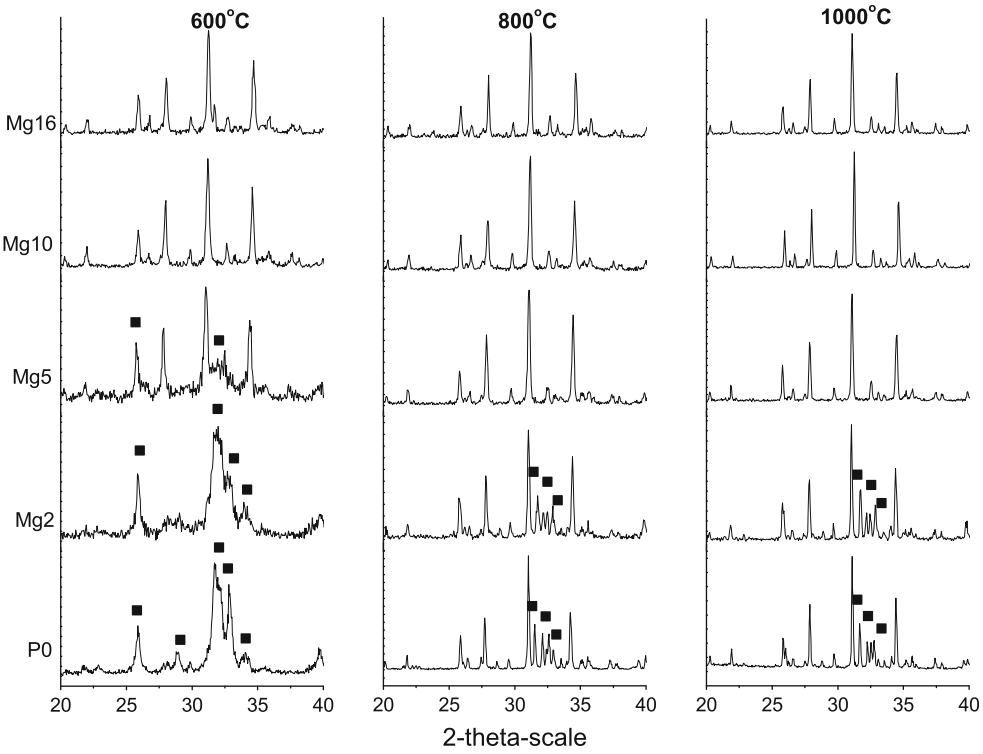

Fig. 2 XRD powder patterns of Mg-modified calcium phosphates at different temperatures (*filled square* HA; *not marked* Mg-β-TCP)

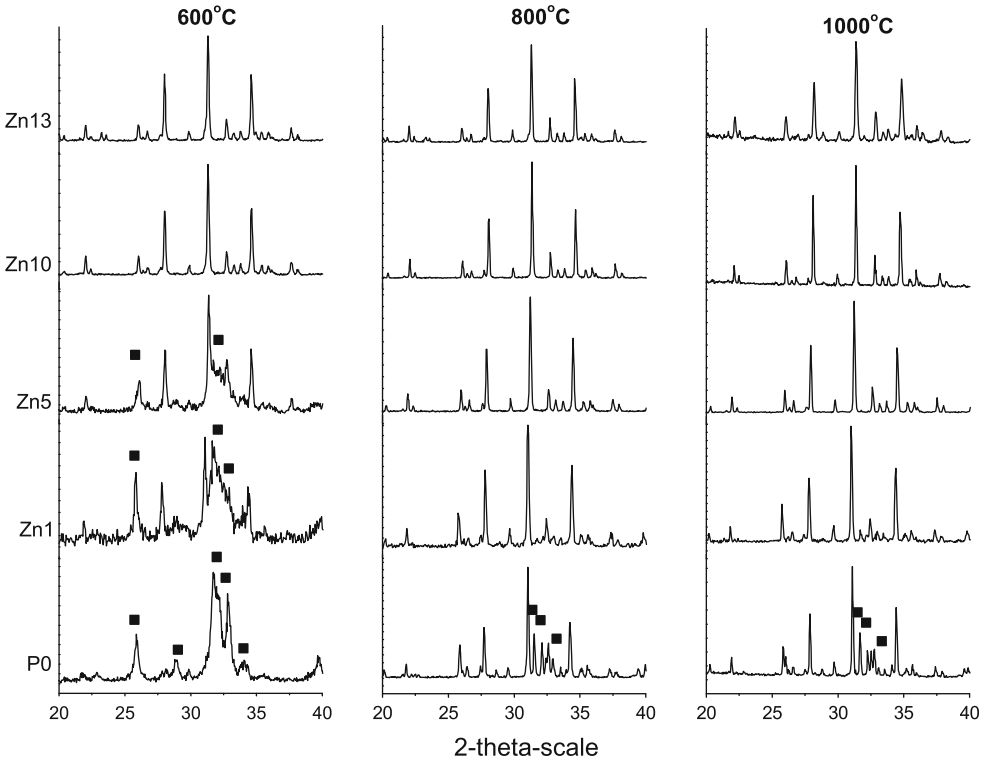

Fig. 3 XRD powder patterns of Zn-modified calcium phosphates at different temperatures (*filled square* HA; *not marked* Zn-β-TCP)

SI > 0); (ii) the increase of the Mg^{2+} ion concentration in the system leads to co-precipitation of additional four metastable magnesium salts and more favorable precipitation of $Ca_9Mg(HPO_4)(PO_4)_6$ (its SI increases); (iii) the only zinc phosphate salt $Zn_3(PO_4)_2{\cdot}4H_2O$ was not calculated to precipitate (SI < 0). This possible co-crystallization of magnesium salts explains the differences between magnesium and zinc samples with lowest and highest Me^{2+} incorporation. The sample Mg2 ($Mg^{2+}/(Ca^{2+}+Mg^{2+}) = 0.02$) has a phase composition similar to SBF modified sample P0

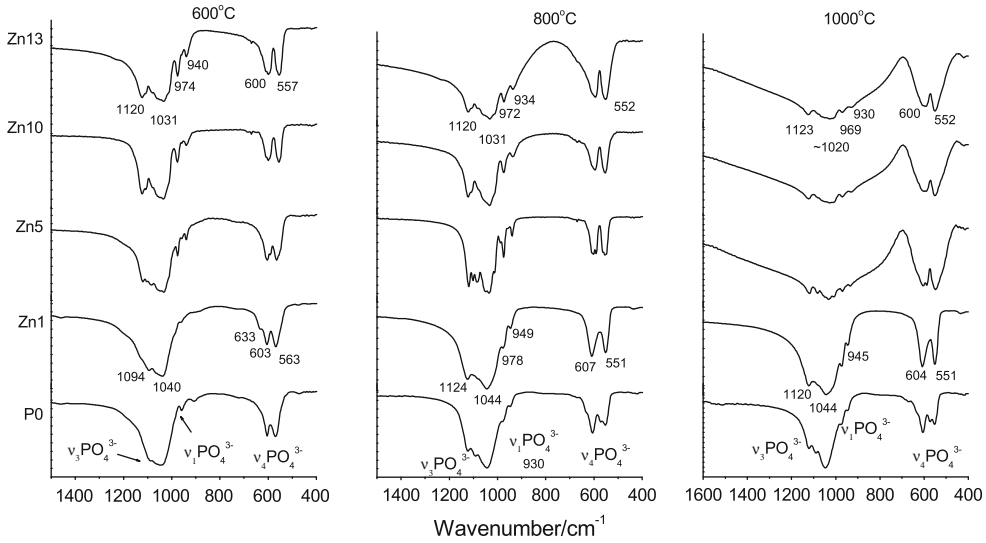

Fig. 4 FT IR spectra of Zn-modified calcium phosphates at different temperatures

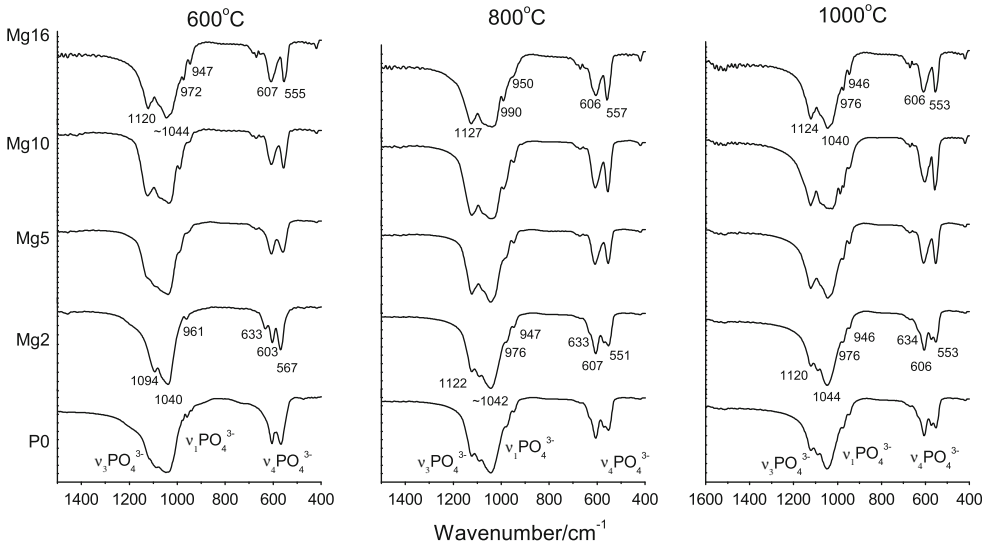

Fig. 5 FT IR spectra of Mg-modified calcium phosphates at different temperatures

even at 1000°C (Fig. 2) whereas the Zn^{2+} ion substitution in the sample Zn1 with a smaller zinc content (Zn^{2+}/(Ca^{2+}+Zn^{2+}) = 0.01) leads to a stable Zn-β-TCP even at 800°C (Fig. 3). The XRD analysis did not register the small amounts of co-crystallized salts even in the case of sample Mg16 with ratio Mg^{2+}/(Ca^{2+}+Mg^{2+}) = 0.16 due to its detectable limits (1–3 wt%). The XRD data (Figs. 2 and 3) revealed that all ion modified amorphous precursors were transformed into HA or Me-β-TCP depending on the additive and its amount as well as on the temperature. Displacements of the major peaks of β-TCP towards lower 2θ values indicate Me^{2+} substitution in their crystal structure. Both Zn^{2+} and Mg^{2+} substitutions stimulated the ACP transformation to HA and Me-β-TCP but the effect was more pronounced in the case of Zn^{2+} substitution. At 600°C, mixtures of HA and Me-β-TCP were observed at Me^{2+}/(Me^{2+} + Ca^{2+}) ratios lower than 0.05 and Zn-β-TCP and Mg-β-TCP for samples with Me^{2+}/(Me^{2+} + Ca^{2+}) ratios higher than 0.05. The crystallinity of SBF modified sample (P0 Fig. 2) was higher than this one for ion-modified sample with Mg^{2+}/(Ca^{2+}+ Mg^{2+}) = 0.02 (Mg2 Fig. 2). Danielchenko et al. [38] have found the transformation of Mg-modified amorphous calcium phosphate into poorly crystalline apatite at 700°C because of different way of precursor preparation and different temperature regime of heating.

Both, the concentration of Mg^{2+} and Zn^{2+} ions and temperature affect the IR spectral characteristics of the studied samples (Figs. 4 and 5). Bands in the range 1040–1120 cm^{-1} are due to antisymmetric P–O stretching mode, while peaks near 960 cm^{-1} to symmetric stretching mode of phosphate group. Peaks near 560 and 600 cm^{-1} arise from the antisymmetric bending mode of phosphate group. Indicative for the presence of hydroxyl groups in hydroxyapatite are peaks at 633 and 3570 cm^{-1}. The absorption bands characteristic for P–O stretching vibrations in β-TCP appeared at 1120, 1100, 1085, 1055, 1035, 976 and around 940 cm^{-1}. IR spectra of

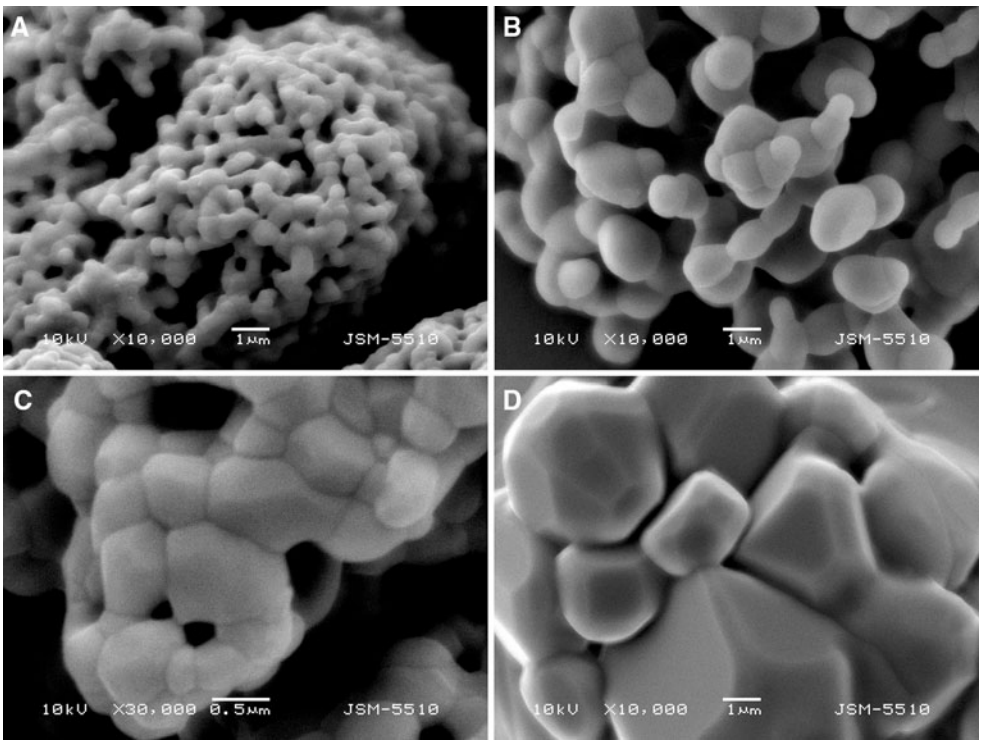

Fig. 6 SEM images of ion-modified calcium phosphates heated at 1000°C. **a** $Mg^{2+}/(Mg^{2+}+Ca^{2+}) = 0.02$, **b** $Mg^{2+}/(Mg^{2+}+Ca^{2+}) = 0.10$, **c** $Zn^{2+}/(Zn^{2+}+Ca^{2+}) = 0.01$, **d** $Zn^{2+}/(Zn^{2+}+Ca^{2+}) = 0.13$

samples with low levels of Zn loadings (Zn1 and Zn5) sintered at 600°C revealed presence of hydroxyapatite evident by the shoulder near 633 cm^{-1} (Fig. 4). The same is observed for the sample Mg2 in all temperature range (Fig. 5). With the increase in ion concentration and temperature the β-TCP phase remains stable. The greater number of peaks observed in the IR spectrum of β-TCP in comparison to HA arises from the existence of three nonequivalent PO_4 tetrahedra in the crystal structure of β-TCP [39]. In addition, ion substitution cause distortion of the structure and probably lowering of the local symmetry, which can be seen at higher ion concentration as increase in number of peaks or broadening of the peaks after heating at 1000°C.

The incorporation of Mg^{2+} and Zn^{2+} ions into the crystal unit cell of the thermodynamically stable HA takes place by Ca^{2+} ion substitution. As the ionic radii of Mg^{2+} and Zn^{2+} are too small in comparison with that of Ca^{2+} the increase of their amount leads to unit cell distortion and volume decrease, established also by Ito et al. [40] and Miyaji et al. [41]. Thus, the structure of Me^{2+} ion modified HA is destabilized and its transformation into more stable Me-β-TCP structure and high temperature Me-α-TCP structure could be expected, but no α-TCP XRD peaks were detected in our experiments even after sintering at 1300°C. Cacciotti et al. [42] also established that ion substitution stabilized the β-TCP structure even at 1600°C. Hyun-Seung Ryu et al. [43] founded that the presence of 1–3% $Ca_2P_2O_7$ delays the phase transformation of β-TCP into α-TCP. It was expected formation of calcium pyrophosphate during heating but its presence was not confirmed by the XRD data. IR spectra also do not provide clear evidence for the presence of pyrophosphate. It could be only assumed for a few samples (P0, Zn13, Mg16, Figs. 4 and 5), where very weak absorption around 920 and 720 cm^{-1} appeared.

The SEM analyzes revealed that Zn^{2+} and Mg^{2+} substitutions influenced the morphology of Me-β-TCP grains (Fig. 6). The sintering at 800–1000°C lead to zinc-modified-β-TCP powders of idiomorphic crystals with average grain sizes of 0.6 μm for Zn1 and 3.8 μm for Zn13 sample (Fig. 6c and d). Magnesium-modified-β-TCP powders with spherical grains covered by blanket and smaller size (0.5 μm average grain size for Mg2 and 1.2 μm for Mg10) were obtained when the $Mg^{2+}/(Mg^{2+} + Ca^{2+})$ ratio was higher than 0.02 (Fig. 6a and b).

4 Conclusions

Amorphous zinc- or magnesium-modified calcium phosphate (ACP) precursors were precipitated by the method of continuous co-precipitation in modified simulated body fluid electrolyte system at pH 8. The different chemical behavior of Zn^{2+} and Mg^{2+} ions in these solutions

determined their different incorporation in the precipitated ACP, predicted also by thermodynamic modeling in the studied system. Powders of zinc- and magnesium-modified-β-TCP and a mixture of Me-β-TCP and HA with a $(Ca^{2+} + Mg^{2+} + Zn^{2+} + Na^{+} + K^{+})/P$ ratio of 1.31–1.4 were obtained after precursors maturation, two steps lyophilization and sintering at 600–1000°C.

The results showed that the temperature as well as the degree of Zn^{2+} and Mg^{2+} ion substitution for Ca^{2+} ions stabilizes the β-TCP structure and the effect was more prononced in the case of zinc substitution. Zn-β-TCP and Mg-β-TCP were observed at 600°C for samples with $Me^{2+}/(Ca^{2+}+Me^{2+})$ ratios higher than 0.05 and mixture of HA and β-TCP calcium phosphates at ratios lower than 0.05. The sintering of Zn^{2+} ion substituted calcium phosphates at 800–1000°C leads to zinc-modified β-TCP with idiomorphic crystals and average grain sizes of 0.6 μm nm for Zn1 sample and 3.8 μm for Zn13 sample. Magnesium-modified β-TCP powders consisted of spherical grains with 0.5 μm average grain size for Mg2 and 1.2 μm for Mg10.

Acknowledgments This work is financially supported by the Bulgarian Ministry of Education, Youth and Science under Projects DTK 02-70/2009 and DCVP-02/2/2009.

References

1. Dorozhkin SV. Calcium orthophosphates in nature, biology and medicine. Materials. 2009;2:399–498.
2. Daculsi G, Bouler JM, LeGeros RZ. Adaptive crystal formation in normal and pathological calcifications in synthetic calcium phosphate and related biomaterials. Int Rev Cytol. 1997;172:129–91.
3. Koroleva LF. Doped nanocrystalline calcium carbonate phosphates. Inorganic Mater. 2010;46:405–11.
4. Stanic V, Dimitrijevic S, Antic-Stankovic J, Mitric M, Jokic B, Plecas IB, Raicevic S. Synthesis, characterization and antimicrobial activity of copper and zinc-doped hydroxyapatite nanopowders. Appl Surf Sci. 2010;256:6083–9.
5. Boanini E, Gazzano M, Bigi A. Ionic substitutions in calcium phosphates synthesized at low temperature. Acta Biomater. 2010;6:1882–94.
6. Sogoa Y, Ito A, Kamo M, Sakurai T, Onuma K, Ichinose N, Otsuka M, LeGeros RZ. Hydrolysis and cytocompatibility of zinc-containing α-tricalcium phosphate powder. Mater Sci Eng. 2004;C24:709–15.
7. Tas C, Bhaduri SB, Jalota S. Preparation of Zn-doped β-tricalcium phosphate (β-$Ca_3(PO_4)_2$) bioceramics. Mater Sci Eng. 2007;C27:394–401.
8. Burchfield CL, Tate AE, Jalota S, Bhaduri SB, Tas AC. Synthesis and in vitro cell culture of Zn-doped calcium phosphates. Eur Cells Mater. 2006;11(1):35.
9. Marchi J, Dantas ACS, Greil P, Bressiani JC, Bressiani AHA, Muller FA. Influence of Mg-substitution on the physicochemical properties of calcium phosphate powders. Mater Res Bull. 2007;42:1040–50.
10. Xue W, Dahlquist K, Banerjee A, Bandyopadhyay A, Bose S. Synthesis and characterization of tricalcium phosphate with Zn and Mg based dopants. J Mater Sci Mater Med. 2008;19:2669–77.
11. Ania CT, Sammons RL, Macaskie LE, Ping Y, Lugg H, Marquis PM. Bacterial biosynthesis of a calcium phosphate bone-substitute material. J Mater Sci Mater Med. 2004;15:403–6.
12. Yamaguchi M. Role of zinc in bone formation and bone resorption. J Trace Elem Exp Med. 1998;11:119–35.
13. Moonga BS, Dempster DW. Zinc is a potent inhibitor of osteoclastic bone resorption in vitro. J Bone Miner Res. 1995;10:453–7.
14. LeGeros RZ, Lin S, Rohanizadeh R, Mijares D, LeGeros JP. Biphasic calcium phosphates: preparation and properties. J Mater Sci Mater Med. 2003;14:201–9.
15. Daculsi G, Laboux O, Malard O, Weiss P. Current state of the art of biphasic calcium phosphate bioceramics. J Mater Sci Mater Med. 2003;14:195–200.
16. Sayer M, Stratilatov AD, Reid JW, Calderin L, Stott MJ, Yin X, MacKenzie M, Smith TJN, Hendry JA, Langstaff SD. Structure and composition of silicon-stabilized tricalcium phosphate. Biomaterials. 2003;24:369–82.
17. Reid JW, Pietak AM, Sayer M, Dunfield D, Smith TJN. Phase formation and evolution in the silicon substituted tricalcium phosphate/apatite system. Biomaterials. 2005;26:2887–97.
18. Tampieri A, Celotti G, Landi E. From biomimetic apatites to biologically inspired composites. Anal Bioanal Chem. 2005;381:568–76.
19. Radin SR, Ducheyne P. Effect of bioactive ceramic composition and structure on in vitro behavior. II. Precipitation. J Biomed Mater Res. 1993;27:35–44.
20. Radin SR, Ducheyne P. Effect of bioactive ceramic composition and structure on in vitro behavior. III. Porous versus dense ceramics. J Biomed Mater Res. 1994;28:1303–9.
21. Petrov OE, Dyulgerova E, Petrov L, Popova R. Characterization of calcium phosphate phases obtained during the preparation of sintered biphase Ca-P ceramics. Mater Lett. 2001;48:162–7.
22. Kokubo T. Surface chemistry of bioactive glass-ceramics. J Non-Cryst Solids. 1990;120:138–51.
23. Sykora V. Chemicko analyticke tabulky. Praha; 1976.
24. Parkhurst DL. User's guide to PHREEQC-A computer program for speciation, reaction-path, advective-transport, and inverse geochemical calculations. U.S. Geological Survey Water-Resources Investigations Report 95-4227, 1995.
25. Todorov T, Rabadjieva D, Tepavitcharova S. New thermodynamic database for more precise simulation of metal species in natural waters. J Univ Chem Technol Metall. 2006;41:97–102.
26. Fernández E, Gil FJ, Ginebra MP, Driessens FCM, Planell JA, Best SM. Calcium phosphate bone cements for clinical applications. Part I: solution chemistry. J Mater Sci Mater Med. 1999;10:169–76.
27. Araújo JC, Sader MS, Moreira EL, Moraes VCA, LeGeros RZ, Soares GA. Maximum substitution of magnesium for calcium sites in Mg-β-TCP structure determined by X-ray powder diffraction with the Rietveld refinement. Mater Chem Phys. 2009;118:337–40.
28. Jalota S, Bhaduri SB, Tas AC. Using a synthetic body fluid (SBF) solution of 27 mM HCO_3^- to make bone substitutes more osteointegrative. Mater Sci Eng C. 2008;28:129–40.
29. Wang H, Lin C, Hu R. Effects of structure and composition of the CaP composite coatings on apatite formation and bioactivity in simulated body fluid. Appl Surf Sci. 2009;255:4074–81.
30. Xin F, Jian C, Jian-Peng Z, Qian W, Zhong-Cheng Z, Jian-Ming R. Bone-like apatite formation on HA/316L stainless steel composite surface in simulated body fluid. Trans Nonferrous Met Soc China. 2009;19:347–52.
31. Rabadjieva D, Gergulova R, Titorenkova R, Tepavitcharova S, Dyulgerova E, Balarew Chr, Petrov O. Biomimetic transformations of amorphous calcium phosphate: kinetic and thermodynamic studies. J Mater Sci Mater Med. 2010;21(9):2501–9.

32. Bigi A, Foresti E, Gandolfi M, Gazzano M, Roveri N. Inhibiting effect of zinc on hydroxylapatite crystallization. J Inorg Biochem. 1995;58:49–58.
33. Betts F, Blumenthal NC, Posner AS, Becker GL, Lehninger AL. Atomic structure of intracellular amorphous calcium phosphate deposits. Proc Natl Acad Sci USA. 1975;72:2088–92.
34. Blumenthal NC, Betts F. Posner AS Stabilization of amorphous calcium phosphate by Mg and ATP. Calcif Tissue Res. 1977;23:245–50.
35. Shannon RD. Revised effective ionic radii and systematic studies of interatomic distances in halides and chalcogenides. Acta Cryst. 1976;A32:751–67.
36. Pearson R. Hard and soft acids and bases. Stroudsburg: Hutchinson Ross Publishing Company; 1973.
37. Klopman G. Chemical reactivity and the concept of charge- and frontier-controlled reactions. J Am Chem Soc. 1968;90:223–34.
38. Danielchenko SN, Protsenko IYu, Sukhodub LF. Some features of thermo-activated structural transformation of biogenic and synthetic Mg-containing apatite with β-tricalciummagnesium phosphate formation. Cryst Res Technol. 2009;44:553–60.
39. de Aza PN, Guitián F, Santos C, de Aza S, Cuscö R, Artús L. Vibrational properties of calcium phosphate compounds. 2. Comparison between hydroxyapatite and β-tricalcium phosphate. Chem Mater. 1997;9:916–22.
40. Ito A, Kawamura H, Otsuka M, Ikeuchi M, Ohgushi H, Ishikawa K, Onuma K, Kanzaki N, Sogo Y, Ichinose N. Zinc-releasing calcium phosphate for stimulating bone formation. Mater Sci Eng. 2002;C22:21–5.
41. Miyaji F, Kono Y, Suyama Y. Formation and structure of zinc-substituted calcium hydroxyapatite. Mater Res Bull. 2005;40:209–20.
42. Cacciotti I, Bianco A. High thermally stable Mg-substituted tricalcium phosphate via precipitation. Ceram Int. 2010;37(1):127–37.
43. Ryu H-S, Youn H-J, Hong KS, Chang B-S, Leeb C-K, Chung S-S. An improvement in sintering property of β-tricalcium phosphate by addition of calcium pyrophosphate. Biomaterials. 2002;23:909–14.